

TABLE 1 Normalized Differential Phase Shift Between Forward and Backward Wave at 3.5 GHz

| θ (deg) | Normalized Differential Phase Shift ($\Delta\beta/k_0$) | |
|-------------------|---|-------------------|
| | $\phi = 0^\circ$ | $\phi = 90^\circ$ |
| 10 | 6.6568e-004 | 4.6596e-004 |
| 20 | 1.3390e-003 | 1.3979e-003 |
| 30 | 2.5118e-003 | 1.5976e-003 |
| 45 | 7.3887e-003 | 0 |
| 60 | 2.3165e-002 | 9.5853e-003 |
| 75 | 5.9642e-002 | 4.6612e-002 |
| 90 | 4.4207e-001 | 8.7796e-002 |

served. This might be due to the propagation constants of the forward and backward waves being degenerate at this angular magnetization. The differential phase shift is considerably higher for the transverse magnetization compared to the normal and longitudinal magnetization cases.

The characteristic impedance (Fig. 7) is observed to reduce with frequency, and the effective dielectric constant of the structure is observed to increase with frequency. At $\phi = 0^\circ$ and an operating frequency of 4 GHz, the characteristic impedance is observed to reduce as θ is varied from 0 to 90° , while the characteristic impedance is observed to increase with θ for 3.5 GHz. The characteristic impedance is observed to increase with θ for $\phi = 90^\circ$ for both 3.5 and 4 GHz. For normal magnetization, the characteristic impedance is observed to be about 30 Ω . Hence, arbitrary orientation may assist in matching with the excitation source impedance, but at 4 GHz, the variation of impedance is not seen much.

The change in differential phase shift with frequency finds many practical applications in microwave integrated circuits like phase shifters.

4. CONCLUSION

A spectral-domain approach is employed in conjunction with matrix methods to estimate the electric and magnetic fields in each layer of the geometry in terms of an exponential matrix characteristic of the material parameters. The resulting integral equation is solved rigorously using the MoM to obtain the dispersion characteristics for both forward and backward waves under arbitrary orientation of dc magnetization. A different orientation of the magnetic field changes the phase constant, current distribution, and characteristic impedance significantly. It is possible to obtain the required phase shift in the microwave band by adjusting the magnetization angle.

REFERENCES

1. M. Tsutsumi and T. Asahara, Microstrip lines using yttrium iron garnet film, IEEE Trans Microwave Theory Tech 38 (1990), 1461–1467.
2. M. Tsutsumi and S. Tamura, Microstrip line filters using yttrium iron garnet film, IEEE Trans Microwave Theory Tech 40 (1992), 400–402.
3. J.L. Tsalamengas, N.K. Uzunoglu, and N.G. Alexopoulos, Propagation characteristics of a microstrip line printed on a general anisotropic substrate, IEEE Trans Microwave Theory Tech MTT-33 (1985), 941–945.
4. K. Okubo, A. Sanada, S. Takenawa, and K. Yamane, FDTD analysis of a microstrip line with YIG film magnetized in arbitrary direction, Asia Pacific Microwave Conf 2000, Sydney, Australia, pp. 357–360.
5. I.Y. Hsia, H.Y. Yang, and N.G. Alexopoulos, Basic properties of microstrip circuit elements on nonreciprocal substrate-superstrate structures, J Electromag Waves Appl 5 (1991), 465–476.

6. D. Mirshekar-Syahkal, Spectral domain method for microwave integrated circuits, Wiley, New York, 1990.
7. T. Itoh and R. Mittra, Spectral-domain method for calculating the dispersion characteristics of microstrip lines, IEEE Trans Microwave Theory Tech MTT-21 (1973), 496–499.
8. G. Tyras, The permeability matrix for a ferrite medium magnetized at an arbitrary direction and its eigen values, IRE Trans Microwave Theory Tech (1959), 176–177.
9. E.L. Tan and S.Y. Tan, Concise spectral formalism in the electromagnetics of bianisotropic media, PIER, 2000, pp. 309–331.
10. G. Leon, R.R. Boix, and F. Medina, Efficient full-wave characterization of microstrip lines fabricated on magnetized ferrites with arbitrarily oriented bias field, J Electromag Waves Appl 15 223–252.
11. M. Tsutsumi, T. Ueda, and K. Okubo, Magnetostatic-wave envelope soliton in microstrip line using YIG-film substrate, IEEE Trans Microwave Theory Tech 48 (2000), 239–402.

© 2001 John Wiley & Sons, Inc.

A BROADBAND MICROSTRIP ANTENNA ARRAY FOR LMDS APPLICATIONS

Soonsoo Oh,¹ Seongho Seo,¹ Mikyoung Yoon,¹ Changyoul Oh,² Eungbae Kim,² and Youngsik Kim¹

¹Department of Radio Sciences and Engineering
Korea University
Seoul 136-701, Korea

²Radio and Broadcasting Technology Laboratory
Electronics and Telecommunications Research Institute
Taejeon 305-350, Korea

Received 25 June 2001

ABSTRACT: In this paper, a broadband 20×20 microstrip antenna array is presented. Once a rectangular microstrip patch antenna with parasitic patches as an element antenna has been optimized at 24.2–26.7 GHz, a parallel-series feed network with minimum feed lengths can be utilized to combine element antennas. From simulation and measurement, the array antenna yields relatively high gains of 26.0–30 dB and narrow 3 dB beamwidths of 4.5–5.1° in the H-plane and 4.1–7.1° in the E-plane, respectively, in an LMDS band. © 2001 John Wiley & Sons, Inc. Microwave Opt Technol Lett 32: 35–37, 2002.

Key words: antennas; microstrip antenna; microstrip antenna arrays
DOI 10.1002 / mop.10084

1. INTRODUCTION

Since a microstrip patch antenna was introduced in 1972 [1], patch antennas have been investigated widely because of their low profile, low weight, lower cost, and easy manufacturing [2, 3]. To broaden the bandwidth of a resonant-type patch antenna, various shapes of microstrip patch antennas have been proposed, such as patch antennas with parasitic elements [4], annular ring antennas [5], and multilayered patches [6]. For LMDS applications, a patch antenna with parasitic elements is one of the best candidates among those antennas because of its simple design and implementation for array element antennas.

Although a hybrid (parallel-series) feed network is well suited for a planar array antenna, each series-fed element antenna phase is not the same. This may be a result of frequency scanning in the LMDS band of 24.2–26.7 GHz [7]. To avoid scanning the spacing of the series-fed element, the antennas have been adjusted. This series feed network has been designed with the Dolph–Chebyshev array method to reduce sidelobes [8].

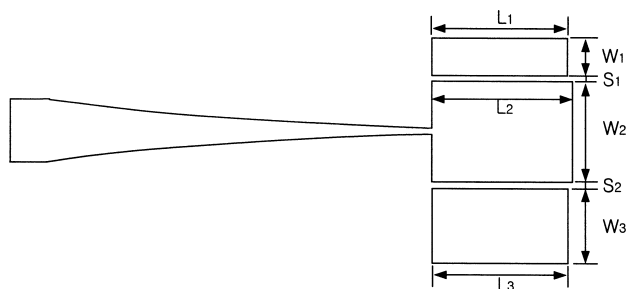


Figure 1 Patch antenna element with parasitic patches

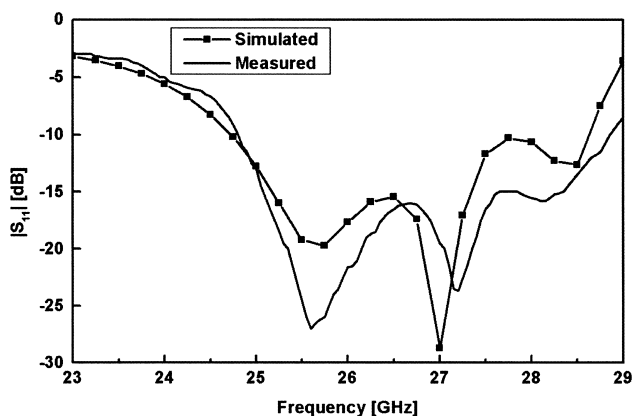


Figure 2 Return loss (S_{11}) of antenna element

2. ELEMENT ANTENNA

Two additional resonators (parasitic patches), which are modified in [8], are placed adjacent to the nonradiating edges of a rectangular patch antenna, as shown in Figure 1. The patch antenna in [8] is not adequate for an element antenna because the dimensions of the E -/ H -plane are larger than $1\lambda_0$. It was fabricated on a substrate with $h = 0.508$ mm (20 mil), $\epsilon_r = 2.2$, and $\tan \delta = 0.0009$. The patch dimensions are $L_1 = L_3 = 3.6$ mm, $L_2 = 3.7$ mm, and $S_1 = S_2 = 0.2$ mm. After determining the width of W_2 , those of W_1 and W_3 have been adjusted to obtain a proper bandwidth using IE3D [9] simulation, and the optimized values of W_1 and W_3 are 1 and 2 mm, respectively. An exponential taper is used to match the input impedance of a single antenna to the $50\ \Omega$ transmission line. The simulated and measured return losses are given in Figure 2. Both curves have similar behaviors of two deeps. The return loss is below -10 dB in a range of 24.5–29 GHz for both. A bandwidth of 12% for $VSWR \leq 2$ is obtained from the simulation, and one of 15% from the measurement. Even though its size is smaller than the structure in [9], the bandwidth is as broad as 15.4% of that in [9].

3. ARRAY ANTENNA

The Dolph–Chebyshev method is used to achieve low side-lobes [8]. For a 20-element array with a -30 dB sidelobe level (SLL), the current distribution from the center patch to the end element is given as 1.00:0.97:0.91:0.83:0.73:0.62:0.50:0.39:0.29:0.33. This current distribution is realized with different impedances of the series feed network. To verify the current distribution of the feed network, the 20×1 linear array antenna was simulated and measured. The 20×20 planar array antenna is depicted in Figure 3. The element spacing is 8.5 mm in the x -direction and 8.35 mm in the

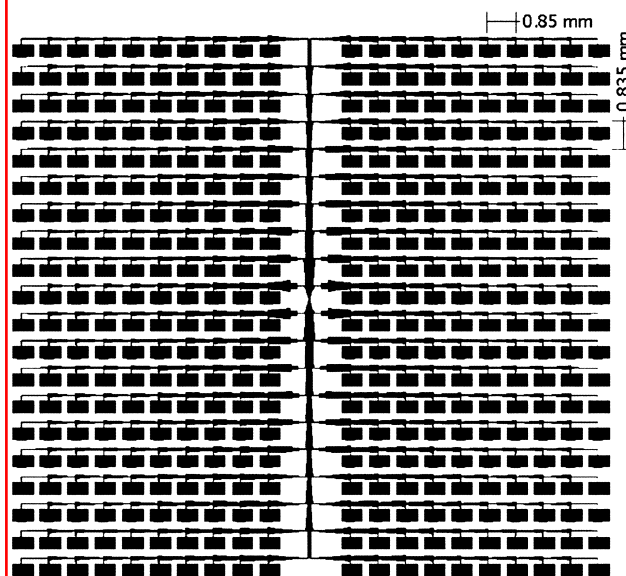


Figure 3 Top view of 20×20 antenna array

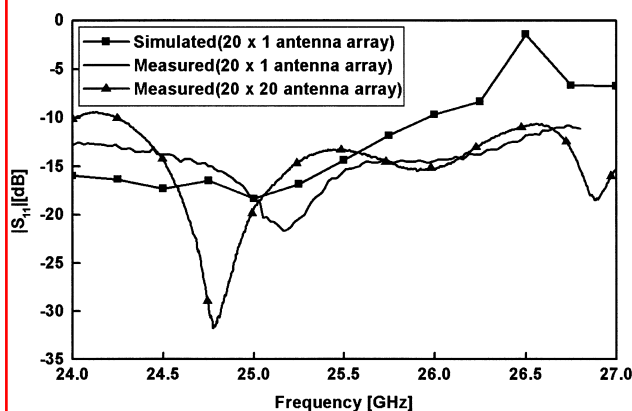


Figure 4 Return loss (S_{11}) of 20×1 and 20×20 antenna arrays

y -direction. The main feed is placed at the center of the array, and this feed results in a 24 mm spacing at the center vertical.

Figure 4 shows the return loss of the 20×1 array antenna and the 20×20 array antenna. The principal E -/ H -plane radiation patterns of the antenna at 25.5 GHz are shown in Figures 5 and 6, respectively. The simulated patterns are similar to the measured ones. While the desired SLL is -30

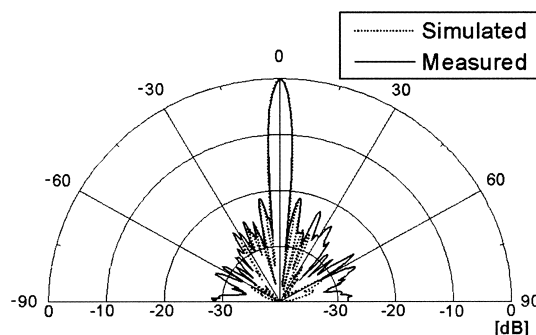


Figure 5 E -plane radiation patterns of 20×20 antenna array at 25.5 GHz

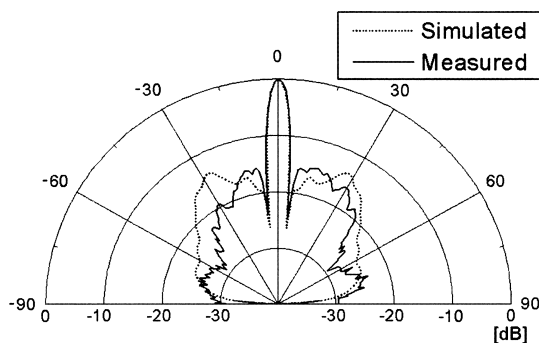


Figure 6 *H*-plane radiation patterns of 20×20 antenna array at 25.5 GHz

TABLE 1 Gain and 3 dB Bandwidth of 20×20 Antenna Array

| Frequency (GHz) | Gain (dBi) | 3 dB Beamwidth (deg) | |
|-----------------|------------|----------------------|-----------------|
| | | <i>H</i> -Plane | <i>E</i> -Plane |
| 24.25 | 26.0 | 4.8 | 5.8 |
| 24.50 | 26.4 | 4.9 | 6.2 |
| 24.75 | 26.8 | 5.0 | 7.1 |
| 25.00 | 27.6 | 5.1 | 5.2 |
| 25.50 | 30.0 | 4.6 | 4.1 |
| 26.00 | 28.3 | 4.6 | 4.6 |
| 26.50 | 27.8 | 4.6 | 4.4 |
| 26.70 | 30.7 | 4.5 | 4.3 |

dB, the measured and simulated ones are -21 dB in the *E*-plane and -15 dB in the *H*-plane, respectively, due to an imperfect power distribution and element spacing of 24 mm along the vertical center feed line.

The gain is 30 dB, and the 3 dB beamwidth is 4.6 and 4.1° in the *E*-/*H*-plane, respectively. The gain and beamwidth of the 20×20 array antenna are summarized in Table 1.

4. CONCLUSION

A microstrip single patch antenna with parasitic patches was developed, and yielded a bandwidth of 15%. A parallel-series feed network with minimum feed lengths was utilized to combine element antennas. A series feed network was designed from the Dolph-Chebyshev method for a -30 dB sidelobe level, while the simulated and measured SLL shows -15 dB due to the feed network. The array antenna provides a gain of 26.0–30.7 dB, and the 3 dB beamwidth is 4.5 – 5.1° in the *H*-plane and 4.1 – 7.1° in the *E*-plane, respectively, at 24.2–26.7 GHz for LMDS applications.

REFERENCES

1. J.Q. Howell, Microstrip antennas, IEEE Antennas Propagat Soc Int Symp, 1972 Dig, pp. 177–180.
2. J.R. James and P.S. Hall, Handbook of microstrip antennas, IEE Electromag Wave Ser 28, Peter Peregrinus, London, England, 1989.
3. D.M. Pozar, Microstrip antennas, Proc IEEE 80 (1992), 79–81.
4. H. Pues, J. Vandensande, and A.V. Capelle, Broadband microstrip resonator antennas, IEEE Antennas Propagat Soc Int Symp, 1978 Dig, pp. 68–69.
5. W.F. Richards, J.D. Qu, and S.A. Long, A theoretical and experimental investigation of annular, annular sector and circular sector microstrip antenna, IEEE Trans Antennas Propagat AP-32 (1984), 864–867.

6. S.A. Long and M.D. Walton, A dual-frequency, stacked circular disc antenna, IEEE Antennas Propagat Soc Int Symp, 1978 Dig, pp. 260–263.
7. F. Lalezari and C.D. Massey, mm-wave microstrip antennas, Microwave J 4 (1987), 87–96.
8. W.L. Stutzman and G.A. Thiele, Antenna theory and design, Wiley, New York, 1998.
9. G. Kumar and K.C. Gupta, Nonradiating edges and four edges gap-coupled multiple resonator broad-band microstrip antenna, IEEE Trans Antennas Propagat AP-33 (1985), 173–178.
10. Zeland Software, Inc., IE3D 6.0, New York, NY, 1999.

© 2001 John Wiley & Sons, Inc.

IMPROVED TUNING ACCURACY OF FIBER GRATING LASERS USING A LINEAR VARIABLE DIFFERENTIAL TRANSFORMER

W. H. Chung,¹ H. Y. Tam,¹ M. S. Demokan,¹ and P. K. A. Wai²

¹ Department of Electrical Engineering

Hong Kong Polytechnic University

Hung Hom, Kowloon, Hong Kong SAR, P.R. China

² Department of Electronic and Information Engineering

Hong Kong Polytechnic University

Hung Hom, Kowloon, Hong Kong SAR, P.R. China

Received 2 July 2001

ABSTRACT: A microprocessor-controlled feedback system using a linear variable differential transformer to measure the compression of a fiber Bragg grating with a view to improve the tuning accuracy of a fiber grating laser is reported. This technique overcomes the large hysteresis of the PZT actuator normally used to compress the grating. A tuning range of about 20 nm with a readout wavelength accuracy of better than ± 0.05 nm was achieved. © 2001 John Wiley & Sons, Inc. Microwave Opt Technol Lett 32: 37–40, 2002.

Key words: fiber lasers; wavelength tuning; fiber Bragg gratings; WDM applications

DOI 10.1002 / mop.10085

INTRODUCTION

Fiber lasers based on fiber Bragg gratings (FBGs) are promising candidates for dense wavelength-division multiplexing (DWDM) systems because of the ease of producing an FBG with a highly accurate and repeatable Bragg wavelength that matches the ITU wavelength grids. Recently, there has been intense interest in employing tunable sources in DWDM systems to use as “spare” components in order to reduce cost by stocking fewer spare lasers. Tunable fiber grating lasers offer an important advantage in this respect because an FBG can be tuned over a large wavelength range in comparison with a semiconductor laser which normally can be tuned over just 1–2 nm.

FBG tuning is generally achieved by using either thermal or mechanical methods [1–5]. The direct thermal tuning technique provides a limited tuning range because of the small wavelength temperature coefficient of an FBG (the typical value is ~ 0.012 nm/ $^\circ\text{C}$), and it is also a very slow tuning technique. Mechanically stretching or compressing an FBG enables a wider tuning range of more than 44 nm [5].

Contract grant sponsor: Research Grants Council of the Hong Kong Special Administrative Region, China

Contract grant number: Project PolyU 5142/97E